Optics & Laser Technology 167 (2023) 109819

Contents lists available at ScienceDirect

Optics and Laser Technology

journal homepage: www.elsevier.com/locate/optlastec

Research Note

# Sensitivity magnification of an interferometric optical fiber sensor with a length-linked virtual reference

Ander Zornoza [a], Jose A. Flores-Bravo [b], Joseba Zubia [b], Joel Villatoro [b,c,*]

[a] Department of the Applied Mathematics, University of the Basque Country UPV/EHU, E-48013 Bilbao, Spain
[b] Department of Communications Engineering, University of the Basque Country UPV/EHU, E-48013 Bilbao, Spain
[c] IKERBASQUE, Basque Foundation for Science, E-48011 Bilbao, Spain

ARTICLE INFO

*Keywords:*
Optical fiber interferometers
Sensitivity amplification
Vernier effect
Optical fiber sensors
Fabry-Perot interferometers
Resonators
Virtual reference

ABSTRACT

Here, it is proposed an alternative to magnify the sensitivity of a single optical fiber interferometric sensor up to two orders of magnitude. The method consists of fabricating the sensing interferometer with a specific length whose spectrum is added to that of a virtual interferometer whose length is linked to the sensing interferometer. In this manner, the spectrum of the sensing and virtual interferometers are made to coincide in a maximum or a minimum. The pattern resulting from said sum has a well-defined envelope that is easy to monitor and correlate with the measurand. Thus, the sensor sensitivity can be magnified as desirable. To demonstrate the method, a microscopic Fabry-Perot interferometer was fabricated and tested as temperature sensor. A temperature sensitivity amplification of 124 times was demonstrated experimentally. The method here proposed may pave the way to practical implementation of the Vernier effect with a single interferometer or resonator.

## 1. Introduction

Interferometric optical fiber sensors are known for their high sensitivity and resolution, which can be determinant to monitor or detect minute changes of a parameter of interest.

In demanding applications, it is desirable to tune or to increase substantially the sensitivity of such devices without compromising their fabrication or interrogation. To this end, the sensor community has proposed different alternatives. A straightforward and successful approach is to increase the length of the interferometer. For example, optical fiber interferometers with arms with hundreds of meters in length have been demonstrated to monitor nanostrain and microseisms [1]. Another example is the ultrasensitive rotation sensor based on the Sagnac effect, which is assembled with several kilometers of polarization maintaining optical fiber [2].

The above approaches may be impractical or impossible to implement with interferometers that are miniature *per se*, with Fabry-Perot interferometers for example. In this case, the sensitivity can be increased by using two interferometers with different lengths (different periods); one of them is used as a reference and the other as a sensor. The idea of cascading two interferometers with different periods is to implement an optical analog of a caliper. For this reason, such an approach is known as the optical Vernier effect, which was demonstrated first with optical resonators [3–5].

In theory, the sensitivity amplification of a sensing system comprising two interferometers with slightly different periods, either in series or in parallel, is huge, see for example Refs. [6–16]. This is so because the envelope of the superposition of two interference patterns shifts much more than a single interference pattern [5,17,18]. However, to track the evolution of the wavelength position of such an envelope, a light source, spectrometer, and passive fiber devices like couplers that operate in an ultra-wide spectral range are necessary. A sensor interrogation system with such requirements is expensive and bulky, hence, impractical. In addition, the fabrication of two interferometers with very specific periods is challenging, even with existing techniques. For these reasons, the sensing systems based on the optical Vernier effect reported so far have been demonstrated only in well-controlled laboratory environments.

Therefore, it is important to investigate new mechanisms to increase the sensitivity of interferometric optical fiber sensors without the referred drawbacks. To this end, the concept of optical harmonic Vernier effect [19] and artificial (or virtual) reference spectrum have been reported [20–28]. However, in such works, the physical length of the sensor and that of the real or virtual reference are arbitrary. For this

* Corresponding author at: Department of Communications Engineering, University of the Basque Country UPV/EHU, E-48013 Bilbao, Spain.
*E-mail address:* agustinjoel.villatoro@ehu.eus (J. Villatoro).

https://doi.org/10.1016/j.optlastec.2023.109819
Received 3 May 2023; Received in revised form 26 June 2023; Accepted 7 July 2023
Available online 15 July 2023

reason, the experimental sensitivity amplification based on the methods proposed in [19,20,21] have not reached the expected theoretical values.

In this work, we propose a simple alternative to magnify the sensitivity of a single interferometer between one and two orders of magnitude. Our approach consists of cascading the sensing interferometer with a virtual or artificial reference. Unlike the methods previously reported [20–28], in our approach, the lengths of the sensing and reference interferometers are not arbitrary; however, they can be calculated easily. The feasibility of our method was demonstrated with a single microscopic Fabry-Perot interferometer that was illuminated with a narrowband light emitting diode. The sensitivity of such interferometer was tunable with the virtual reference; sensitivity amplification of two orders of magnitude as compared with that of a single interferometer was demonstrated experimentally.

The concepts and signal processing proposed here can be implemented with literally any type of two-beam or two-mode interferometer and even with resonators. The sensitivity of such measuring devices can be substantially enhanced. Thus, we believe that the approach and results reported here may pave the way for practical applications of the optical Vernier effect with resonant or interferometric sensors.

## 2. Theoretical analysis

The transfer function of a two-beam or two-mode interferometric sensor can be expressed as:

$$T = A + B\cos(2\pi\Lambda/\lambda) \tag{1}$$

where $A$ and $B$ are terms that depend exclusively on the intensities of the interfering beams or modes, $\lambda$ is the wavelength of the excitation optical source, and $\Lambda$ can be either $\Lambda = nd_s$, $\Lambda = \Delta nd_s$, $\Lambda = 2nd_s$ or $\Lambda = 2\Delta nd_s$, depending if the transmission or reflection is monitored and if the interference is between beams or modes. In these expressions, $n$ is the refractive index of the optical fiber or cavity, and $\Delta n$ is the difference between the effective refractive indices of the interfering modes. $d_s$ is the physical length of the interferometer. When the interference is between two beams, $\Lambda$ is the optical path length or the optical distance.

In an interferometric sensor, changes of the measurand being sensed, e.g., temperature, strain, refractive index, etc. can alter $\Lambda$. This may result in a picometer shift of the interference pattern expressed by Eq. (1). Therefore, a change in the measurand can be deduced from the shift of the transmission or reflection spectrum of the interferometer. To do so, interferometric sensors are interrogated with a wide spectrum light source and an optical spectrum analyzer or with a tunable laser and a photodetector. To quantify the interference pattern shift, the wavelength position of the maxima of the pattern can be monitored.

The maxima of Eq. (1) appear at wavelengths that fulfill the following equation [29],

$$2\pi\Lambda/\lambda = 2\pi k \tag{2}$$

where $k$ is an integer.

Now, let us suppose that we take advantage of the periodic nature of interferometers and design them with lengths given by $d_s = k\lambda_c/p$, where $\lambda_c$ is the wavelength where we want an interference pattern maximum and $p$ can be either $n$, $2n$, $\Delta n$ or $2\,\Delta n$ depending on the type of interferometer and how it is interrogated (in transmission or in reflection mode).

Let us define $L_B = \lambda_c/p$. This means, we propose to design the interferometers with a physical length that fulfills the following condition:

$$d_s = kL_B \tag{3}$$

Note that the previous expression is valid whether the interferometer is a low-finesse Fabry-Perot, a Sagnac, Mach-Zehnder, Michelson, or modal one. The transmission or reflection spectrum of such interferometers is periodic in wavelength.

According to Eq. (3), to calculate the length of a sensing interferometer, the only thing needed is the value of $n$ or $\Delta n$. This means, the refractive index of the cavity (in case of a Fabry-Perot interferometer), or the refractive index of the fiber core. In case of modal interferometers; the effective refractive indices of the interfering modes must be calculated.

It is important to point out that the above analysis is not valid if more than two beams or modes participate in the interference.

To implement an optical analog of a caliper with two interferometers, we propose a reference interferometer of the same type of the sensing interferometer but with a length that is proportional to $L_B$. The transfer function of the reference interferometer can also be expressed with Eq. (1). In this manner, both interferometers will have a maximum at $\lambda_c$.

If the sensing and reference interferometers are in parallel, the transfer function ($T_V$) of the cascade will be the sum of the individual transfer functions [10]. After normalization we get,

$$T_V = \cos[\pi(\Lambda_s + \Lambda_r)/\lambda]\cos[\pi(\Lambda_s - \Lambda_r)/\lambda] \tag{4}$$

In Eq. (4), $\Lambda_s = pd_s$ and $\Lambda_r = pd_r$, where $d_s$ and $d_r$ are, respectively, the lengths of the sensing and reference interferometers.

In the composed spectrum given in Eq. (4), the sum of $\Lambda_s$ gives the high frequency component and the subtraction of the same gives the low frequency component, which is the envelope of the composed spectrum. The maximum of the envelope is also located at $\lambda_c$ as $d_s$ and $d_r$ are multiple of $L_B$.

The optical analog of the Vernier effect is especially interesting for sensing applications since the sensitivity of the sensing system can be magnified by a factor $M$, which has been widely discussed in the literature. The sensitivity magnification is [5,10,17,19].

$$M = \Lambda_s/|\Lambda_s - \Lambda_r| \tag{5}$$

The above equation suggests that by having two interferometers with very similar lengths or periods, the sensor sensitivity can be increased a large number of times. However, when $d_s$ and $d_r$ are similar, it is difficult to monitor the wavelength position of the envelope, as it can be ultrabroad.

One way to ensure that the envelope's maximum is tracked is to design the interferometers so that their $\Lambda_s$ fulfill the following condition [29]:

$$\pi|\Lambda_s - \Lambda_r|/\lambda_c = \pi m \tag{6}$$

where $m$ is an integer. Equation (6) is satisfied when the length of the reference interferometer is as follows

$$d_r = (k \pm m)L_B \tag{7}$$

This means that the reference interferometer can be $mL_B$ times longer or shorter than the sensing one. In either case, the maximum of the envelope will be at $\lambda_c$ in which a maximum of both sensing and reference interferometers coincide.

If we chose to track the minimum of the envelope as proposed in [14,30–32], the condition given in Eq. (6) changes, as on the right hand side, we will have $\pi(m+1/2)$ [33]. In this case, $d_r = [k \pm (m+1/2)]L_B$. It means that while the sensor has a maximum at $\lambda_c$, the reference interferometer has a minimum in that wavelength. Thus, the envelope has a minimum at $\lambda_c$ that is also easy to monitor and correlate with a measurand. Thus, the analysis is analogous for the case of tracing the maximum or the minimum dip of a sinusoidal spectrum. The value of $m$ will change, from an integer to an integer plus a half, in the maximum or minimum tracing cases, respectively.

Note that if in Eq. (5), we substitute $\Lambda_s$ and $\Lambda_r$ with the values of $d_s$ and $d_r$ given in Eq. (3) and Eq. (7), the sensitivity magnification is reduced to the following simple expression:

$$M = k/m \tag{8}$$

According to Eq. (8), any sensitivity amplification can be achieved; it only depends on the selected values of $k$ and $m$. The absolute maximum value of $M$ can be achieved when $m = 1$; this is to say, when the difference in length between the sensing and reference interferometer is $L_B$.

It can be noted that according to Eq. (8), $M$ can only have finite and reachable values, which suggests practical implementation of the concepts here proposed. If maximum values of $M$ are desirable, the period of the sensing interferometer should be as short as possible.

We would like to point out that the 'resolution' of a caliper is calculated with a ratio between one division of the primary scale over the number of divisions of the Vernier (auxiliary) scale. In a caliper, the larger the number of divisions of the Vernier scale the higher the resolution. This is what Eq. (8) suggests, higher sensitivity magnification, hence higher resolution, can be achieved when the interference patterns have a large number of maxima and minima.

The values of $k$ and $m$ have great implications on the period or Free Spectral Range ($FSR_{env}$) of the envelope and on the measuring range of the sensor, as there is a tradeoff between these two factors and the sensitivity magnification. For great $m$ values, the sensitivity amplification will be smaller, but the $FSR_{env}$ will be shorter, which makes easier to trace the maximum of the envelope. On the other hand, a large sensitivity amplification (a great $M$ value) may reduce substantially the total measuring range. Furthermore, the detection limit can be degenerated by using the Vernier effect, especially for great $M$ values [34].

We have that the period of the envelope, based on the analysis reported in [5,7,18], combined with Eqs. (3) and (7) is reduced to the following simple expression:

$$FSR_{env} = \lambda_c / m \tag{9}$$

Therefore, for low $m$ values, the $FSR_{env}$ can be thousands of nanometers, which imposes the use of an ultra-broad light source and a suitable spectrometer to follow the evolution of the envelope. For this reason, some authors have limited the $FSR_{env}$ to the measuring spectral range for a correct trace of the position of the maximum of the envelope, see for example [16,19,27,35]. In our case, this is not the situation since the envelope can be centered at $\lambda_c$. A Spline fit over local maxima is successful if the envelope has at least three local maxima in the interrogation wavelength range.

The free spectral range of the sensing interferometer, following the analysis discussed in [5,7,18] with Eq. (3), is:

$$FSR_s = \lambda_c / k \tag{10}$$

Thus, according to Eqs. (9) and (10), $FSR_{env} > 3FSR_s$ means that $M > 3$. This is the minimum sensitivity magnification that can be achieved with the optical Vernier effect, for a correct tracing of the maximum or minimum dip, with at least three maxima per envelope.

Let us now analyze the measuring range that can be achieved. We must first define the measuring range of a sensor, which is given by:

$$\Delta\Lambda_s = FSR_s / S_s \tag{11}$$

with $S_s$ the sensitivity of the sensing interferometer. The $\Lambda_{env}$ is the range in which the unique maximum or maxima of the envelope can be traced. Note that a great sensitivity magnification will drastically reduce the $\Lambda_{env}$, since a large change of the measurand will shift the envelope outside the measuring spectral range ($\Delta\lambda$), which is the spectral width of the light source used to interrogate the interferometers. If we chose a great $m$ to ensure that $FSR_{env} < \Delta\lambda$, the measuring range is not altered. On the contrary, when $FSR_{env} > \Delta\lambda$, the maximum change of the measurand that can be detected will be severely limited.

We can define

$$\Delta\Lambda_{env} = \Delta\lambda / S_{env} \tag{12}$$

where $S_{env}$ is the sensitivity that is achieved when the envelope is monitored. Therefore, we have:

$$\Delta\Lambda_s / \Delta\Lambda_{env} = M(FSR_s / \Delta\lambda) \tag{13}$$

Equation (13) indicates that the measuring range of a sensing system based on the optical Vernier effect is reduced $M$ times.

The above theoretical analysis allows us to design a sensing system based on two interferometers in parallel with a sensitivity amplification defined by Eq. (8) and maximum possible measuring range.

Next, we discuss some examples and experimental results.

## 3. Results and discussion

In the previous section, we have discussed the relation between the lengths of the sensing and reference interferometers to implement a functional Vernier effect. In some situations, it will be difficult to center the two interferometers at $\lambda_c$ because it will imply manufacturing the interferometers with an error well below $L_B$. This can be about a few nanometers for Fabry-Perot interferometers (FPI). Thus, herein we propose to build a virtual reference interferometer, which is of the same type of the sensing interferometer, but with a length that is linked to the sensing interferometer, see Eq. (7).

It is important to point out that the use of an artificial reference spectrum has been recently proposed by other authors, see for example [20–28]. However, in those works, the lengths (periods) of the real sensor and that of the artificial reference did not have any specific relationship. In our case, the sensing device and the virtual reference have lengths that fulfill Eqs. (3) and (7). The technique reported here is centered on magnifying and pushing the limit of the sensitivity of a single interferometric sensor with a simple signal processing. Limiting factors such as the signal demodulation jumps can be overcome by combining with existing techniques such as the ones reported in [36].

The interferometric sensor can be interrogated as usual, with a narrow-band light source and a conventional optical spectrum analyzer (OSA). The measured spectrum is added to a virtual reference that is calculated with the transfer function of the sensing interferometer but with a length that fulfills the condition stated in Eq. (7). The composed spectrum is then calculated with Eq. (4). By tuning the length of the virtual interferometer, the sensitivity amplification and measuring range of the sensor can also be tuned. Furthermore, the technique here proposed allows a simple data processing of the measured spectrum through Spline fit over local maxima and allows reducing the dependence on the spectral wavelength range of the light source and passive devices through normalization.

To demonstrate the feasibility of our approach, we fabricated some low-finesse FPIs whose cavities where made of polymer. The fabrication procedure and transfer function of the FPI are described in detail in [37]. To allow a better understanding of the sensor, in Fig. 1, we show a schematic representation of the device and its interrogation. The interference in said device is between two beams, one is reflected from the


**Fig. 1.** Schematic representation of a Fabry-Perot interferometer and its interrogation which comprises a super-luminescent light emitting diode (SLED), a 2x1 coupler, and an optical spectrum analyzer (OSA). The signal processing is done with a virtual reference. $k$ and $L_B$ are defined in the text; $n_p$ is the refractive index of the cavity.

fiber-polymer interface and the other from the polymer-external medium interface. The spectral width of the super-luminescent light emitting diode (SLED) used in the interrogation system had a $\Delta\lambda = 140$ nm. The central or peak wavelength of the SLED was 1550 nm.

In the FPI shown in Fig. 1, $L_B = \lambda_c/(2n_p)$, where $n_p$ is the refractive index of the polymer that fills the cavity. In our case, $n_p = 1.5409$ at 1550 nm. Thus, according to Eq. (3), $L_B = 0.503\mu m$ at that wavelength. In the following analysis, the cavity length of the virtual FPI will be considered to be longer, *i. e.* $d_r = d_s + mL_B$.

A sample was fabricated with $k = 258$, so, with $d_s \approx 129.77$ μm. As an application example, the sample was exposed to temperatures from 20 to 46 °C. Fig. 2 shows the normalized interference patterns of the FPI at different temperatures. From the experimental data, the temperature sensitivity of the device was found to be −75.5 pm/°C. The shift of the interference pattern was to shorter wavelengths due to the expansion of the polymer [37].

In order to monitor all the aforementioned temperature range with an enhanced sensitivity, we calculated a virtual FPI for with the transfer function provided in [37]. A maximum of the sensing and virtual FPI were made to coincide at 1547.26 nm, which happened when the temperature was 34 °C. Thus, by following the theoretical analysis discussed in section II, the length of the virtual FPI was $d_r = 137.82$ μm, when $m = 16$ and $d_r = 132.29$ μm, when $m = 5$. Under these conditions, the sensitivity magnifications were expected to be $M \approx 16$ and $M \approx 52$, respectively.

Fig. 3 displays the normalized interference patterns of a FPI with $d_s \approx 129.77$ μm and that of the virtual reference calculated when $m = 16$. The sum of both patterns and the envelope of the composed spectrum are also shown in the figure. The evolution of the envelope as a function of temperature is shown in Fig. 4(a) and the calibration curves are shown in Fig. 4(b). The fitting equations of the experimental points shown in stars, empty circles, and solid dots were, respectively T = -13.25 λ + 20768.45, T = 0.85λ-1279.53, T = 0.27λ-383.97. In all cases, $T$ is temperature in degree Celsius and λ is in nanometers. From Fig. 4(b), the temperature sensitivities were found to be 1177.4 pm/°C and 3697.5 pm/°C, when $m$ was 16 and 5, respectively. This means, the sensitivity magnifications experimentally obtained were 16 (when $m = 16$) and 51 (when $m = 5$), which are in good agreement with the theoretical values. It is interesting to note that the above sensitivity amplifications were achieved without reducing the temperature measuring range.

A second sample was fabricated to increase the temperature sensitivity of the sensor as much as possible. A FPI was built with a polymer cavity with $d_s = 177.86$ μm, i.e., $k = 354$. In this case, the minimum of the envelope was correlated with temperature. To enhance the temperature sensitivity by two orders of magnitude, the length of the cavity of the virtual FPI was calculated as $d_r = d_s + (2 + 1/2)L_B$. This means, $d_r$

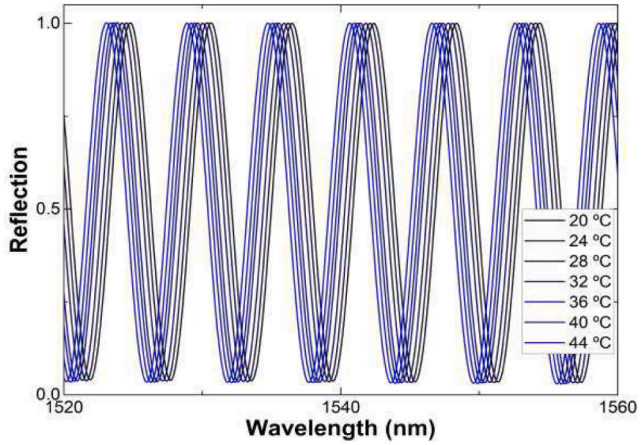


**Fig. 2.** Reflection spectra of a FPI ($d_s = 129.77$ μm) at different temperatures indicated in the graph.

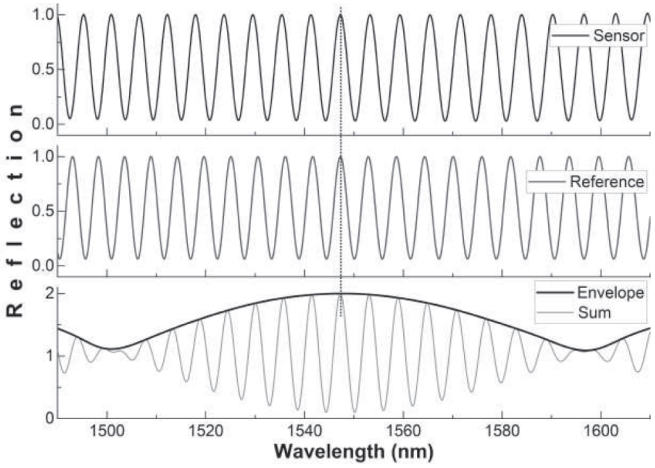


**Fig. 3.** Normalized spectra of a fabricated FPI sensor with $d_s = 129.77$ μm, of the virtual reference calculated with $m = 16$ ($d_s = 137.82$ μm), and of the sum of both spectra. The thick continuous line is the envelope. The dotted vertical line is the maxima in which sensor and virtual reference are made to coincide.

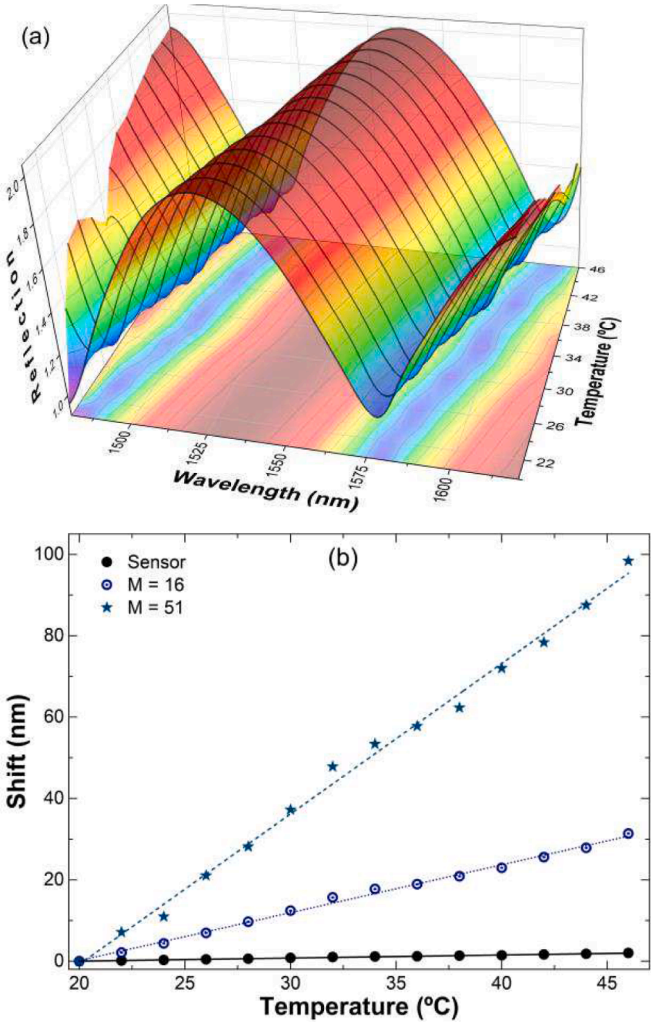


**Fig. 4.** (a) Evolution of the normalized envelope shown in Fig. 3 as a function of temperature. (b) Shift of the interference pattern of a single sensor (solid dots) and shift of the envelope (hollow dots or stars) as a function of temperature for two different virtual references. In all cases the sensing FPI had $d_s = 129.77$ μm.

= 181.36 μm.

In Fig. 5, we show the reflection spectrum of the fabricated sensor and of the virtual reference as well as the resulting sum of both spectra and its envelope. Note that in this case, a minimum of the reflection spectrum of the virtual interferometer is made to coincide with a maximum of the spectrum of the sensing interferometer. Consequently, the envelope has a minimum at such wavelength, which is indicated in Fig. 5 with the vertical dotted line.

The shape and evolution of the envelope at different temperatures are shown in Fig. 6(a). The shift of the interference pattern of the FPI and the shift of the envelope as a function of temperature are shown in Fig. 6 (b). The fitting equation for the case shift of the envelop is T(℃) = -7.31λ (nm) + 11449.15, while the fitting equation of the shift of the interferometer is T(℃) = 0.06λ(nm)-51.48. Thus, the temperature sensitivity through the Vernier effect was found to be 16899.8 pm/°C. This means the temperature sensitivity magnification that was obtained experimentally was 124. The theoretical value was 142. The discrepancy between the expected and measured sensitivity amplifications may be due to imperfections of the real sample, which is referenced with an ideal one. It can be noted that the measurement range was reduced to 4 °C.

The huge sensitivity magnification that can be experimentally achieved with our Fabry-Perot interferometer and signal processing can be crucial to detect, for instance, trace amount of chemical substances as they can induce minute refractive index changes of the polymeric cavity of the FPI [17].

It is worth mentioning that the about experimental sensitivity amplifications were obtained with a simple interrogation system. The light source (an SLED) and the optical fiber coupler used in the experiments were narrow band and of low cost. Such components do not comprise the overall cost of a sensor.

Our results suggest that it is feasible to implement the Vernier effect with a single and compact interferometer and a simple sensor interrogation system. The sensor sensitivity can be amplified one order of magnitude without comprising the measuring range. Higher sensitivity amplification is possible but the measuring range is reduced.

## 4. Conclusions

In this work, we have demonstrated that the Vernier effect can be implemented with a single interferometer and virtual reference that is easy to calculate. We have provided simple formulae to calculate the lengths of the sensor and the virtual reference.

Since a virtual reference has no fabrication errors or dependence on the external environment, it can be designed to tune the sensitivity amplification of an interferometric sensor. For example, the sensor sensitivity can be amplified between a few times to two orders of magnitude.

An important advantage of the approach proposed here is that the interrogation system of the sensor and the virtual reference is as simple as that of a single interferometer. Thus, it can be implemented with widely available components.

It seems feasible to implement a multi-point sensing system with several interferometers and a single or multiple virtual references. Thus, the analysis and results reported may pave the way to practical applications of the Vernier effect with optical fiber interferometers.

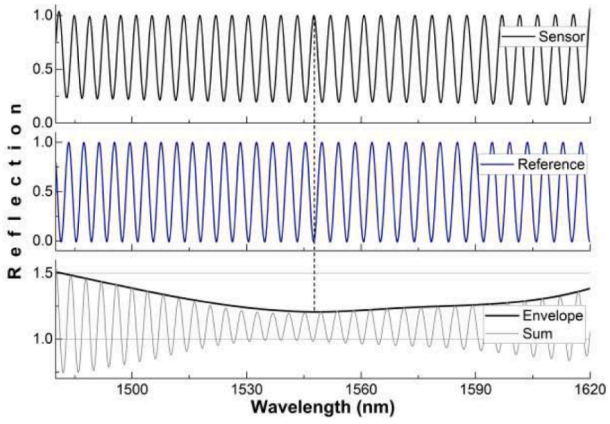


**Fig. 5.** Normalized reflection spectrum of a sensor where $d_s$ = 177.86 μm, of a virtual reference calculated with $m$ = 2.5, and resulting spectrum of the sum of the sensor plus reference spectra. The envelope is shown with a thick solid line. In this case, a minimum of the reference is made to coincide with a maximum of the sensor.

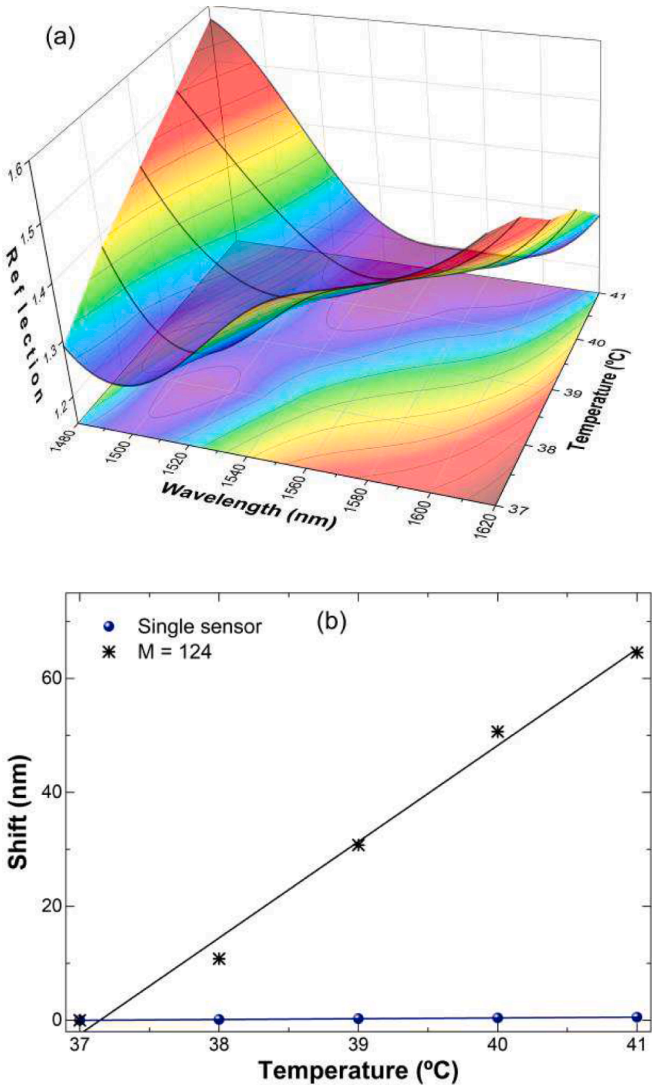


**Fig. 6.** (a) Evolution of the normalized envelope shown at the bottom of Fig. 5 as a function of temperature. (b) Shift of the envelope shown in (a) and shift of the interference pattern of a single FPI as a function of temperature. The solid lines are linear fittings to the experimental points. In this case, the temperature sensitivity was amplified 124 times.

## CRediT authorship contribution statement

**Ander Zornoza:** Formal analysis, Writing – original draft, Conceptualization, Methodology. **Jose A. Flores-Bravo:** Validation, Methodology. **Joseba Zubia:** Funding acquisition, Project administration. **Joel Villatoro:** Formal analysis, Investigation, Writing – review & editing.

## Declaration of Competing Interest

The authors declare that they have no known competing financial interests or personal relationships that could have appeared to influence the work reported in this paper.

## Data availability

Data will be made available on request.

## Acknowledgements

This work was supported in part by the grants PDC2022-133885-100, I + D + i/PID2021-122505OB-C31, TED2021-129959B-C21, funded by MCIN/AEI/10.13039/501100011033, by "ERDF A way of making Europe", by the "European Union Next Generation EU/PRTR" and by Gobierno Vasco/Eusko Jaurlaritza (IT1452-22); ELKARTEK (KK2021/00082, KK2021/00092, KK2021/108, and KK2022/00080).

## References

[1] M.A. Zumberge, W. Hatfield, F.K. Wyatt, Measuring seafloor strain with an optical fiber interferometer, Earth and Space, Science 5 (2018) 371–379, https://doi.org/10.1029/2018EA000418.
[2] H.C. Lefèvre, The fiber-optic gyroscope: challenges to become the ultimate rotation-sensing technology, Opt. Fiber Technol. 19 (2013) 828–832, https://doi.org/10.1016/j.yofte.2013.08.007.
[3] G. Griffel, Vernier effect in asymmetrical ring resonator arrays, IEEE Photon. Technol. Lett. 12 (2000) 1642–1644, https://doi.org/10.1109/68.896334.
[4] D. Dai, Highly sensitive digital optical sensor based on cascaded high-Q ring-resonators, Opt Express. 17 (2009) 23817, https://doi.org/10.1364/oe.17.023817.
[5] T. Claes, W. Bogaerts, P. Bienstman, Experimental characterization of a silicon photonic biosensor consisting of two cascaded ring resonators based on the Vernier-effect and introduction of a curve fitting method for an improved detection limit, Opt Express. 18 (2010) 22747, https://doi.org/10.1364/oe.18.022747.
[6] M. Quan, J. Tian, Y. Yao, Ultra-high sensitivity Fabry-Perot interferometer gas refractive index fiber sensor based on photonic crystal fiber and Vernier effect, Opt Lett. 40 (2015) 4891, https://doi.org/10.1364/ol.40.004891.
[7] H. Lin, F. Liu, H. Guo, A. Zhou, Y. Dai, Ultra-highly sensitive gas pressure sensor based on dual side-hole fiber interferometers with Vernier effect, Opt Express. 26 (2018) 28763, https://doi.org/10.1364/oe.26.028763.
[8] J. Zhang, H. Liao, P. Lu, X. Jiang, X. Fu, W. Ni, D. Liu, J. Zhang, Ultrasensitive Temperature Sensor with Cascaded Fiber Optic Fabry-Perot Interferometers Based on Vernier Effect, IEEE Photonics J. 10 (2018) 1–11, https://doi.org/10.1109/JPHOT.2018.2865449.
[9] J. Deng, D.N. Wang, S. Member, Ultra-Sensitive Strain Sensor Based on Femtosecond Laser Inscribed In-Fiber Reflection Mirrors and Vernier Effect, J. Lightwave Technol. 37 (2019) 4935–4939, https://doi.org/10.1109/JLT.2019.2926066.
[10] T. Nan, B. Liu, Y. Wu, J. Wang, Y. Mao, L. Zhao, T. Sun, J. Wang, Ultrasensitive strain sensor based on Vernier- effect improved parallel structured fiber-optic Fabry-Perot interferometer, Opt Express. 27 (2019) 17239, https://doi.org/10.1364/oe.27.017239.
[11] Y. Wu, B. Liu, J. Wu, L. Zhao, T. Sun, Y. Mao, T. Nan, J. Wang, A Transverse Load Sensor with Ultra-Sensitivity Employing Vernier-Effect Improved Parallel-Structured Fiber-Optic Fabry-Perot Interferometer, IEEE Access 7 (2019) 120297–120303, https://doi.org/10.1109/ACCESS.2019.2933561.
[12] C. Lang, Y. Liu, Y. Liao, J. Li, S. Qu, Ultra-Sensitive Fiber-Optic Temperature Sensor Consisting of Cascaded Liquid-Air Cavities Based on Vernier Effect, IEEE Sens J. 20 (2020) 5286–5291, https://doi.org/10.1109/JSEN.2020.2970431.
[13] R. Pan, W. Yang, L. Li, Y. Yang, X. Yu, J. Fan, S. Yu, Y. Xiong, L. Zhang, High-sensitive fiber-optic pressure sensor based on Fabry-Perot interferometer filled with ultraviolet glue film and Vernier effect, Opt. Fiber Technol. 67 (2021), 102710, https://doi.org/10.1016/j.yofte.2021.102710.
[14] Y. Zhao, M. Dai, Z. Chen, X. Liu, M.S.A. Gandhi, Q. Li, H.Y. Fu, Ultrasensitive temperature sensor with Vernier-effect improved fiber Michelson interferometer, Opt Express. 29 (2021) 1090, https://doi.org/10.1364/oe.415857.
[15] L. Hou, Y. Li, Y. Fu, J. Yang, W. Xu, X. Song, J. Li, Y. Liu, L. Ran, Ultra-Sensitive Optical Fiber Humidity Sensor via Au-Film-Assisted Polyvinyl Alcohol Micro-Cavity and Vernier Effect, IEEE Trans Instrum Meas. 71 (2022), https://doi.org/10.1109/TIM.2021.3139694.
[16] A.D. Gomes, J. Kobelke, J. Bierlich, J. Dellith, M. Rothhardt, H. Bartelt, O. Frazão, Giant refractometric sensitivity by combining extreme optical Vernier effect and modal interference, Sci Rep. (2020) 1–14, https://doi.org/10.1038/s41598-020-76324-7.
[17] Y. Liu, X. Li, Y. nan Zhang, Y. Zhao,, Fiber-optic sensors based on Vernier effect, Measurement (Lond) 167 (2021), https://doi.org/10.1016/j.measurement.2020.108451.
[18] L. Jin, M. Li, J.J. He, Highly-sensitive silicon-on-insulator sensor based on two cascaded micro-ring resonators with vernier effect, Opt Commun. 284 (2011) 156–159, https://doi.org/10.1016/j.optcom.2010.08.035.
[19] A.D. Gomes, M.S. Ferreira, J. Bierlich, J. Kobelke, M. Rothhardt, H. Bartelt, O. Frazão, Optical harmonic vernier effect: A new tool for high performance interferometric fibre sensors, Sensors (Switzerland). 19 (2019) 1–18, https://doi.org/10.3390/s19245431.
[20] X. Fang, W. Zhang, J. Li, C. Lin, Z. Chen, M. Zhang, S. Huang, D. Lu, M. Wan, X. Qiu, Signal processing assisted Vernier effect in a single interferometer for sensitivity magnification, Opt Express 29 (2021) 11570, https://doi.org/10.1364/oe.418783.
[21] F. Zhang, B. Qi, B. Su, O. Xu, Y. Qin, High Sensitivity Hollow-Core Fiber Strain Sensor Based on Signal Processing Assisted Vernier Effect, IEEE Photon. Technol. Lett. 34 (2022) 1050–1053, https://doi.org/10.1109/LPT.2022.3199576.
[22] Y. Zhao, et al., Silicone Rubber Coated Non-Adiabatic Tapered Fiber Combined With Online Vernier Interferometer for Temperature Detection, IEEE Sens. J. 22 (9) (1 May 1, 2022,) 8530–8536, https://doi.org/10.1109/JSEN.2022.3162931.
[23] C. Zhu, J. Huang, High-sensitivity optical fiber sensing based on a computational and distributed Vernier effect, Opt Express 30 (2022) 37566, https://doi.org/10.1364/OE.463619.
[24] Y. Guan and X. Dong. "Reconfigurable highly-sensitive interferometric sensor with Vernier effect and a virtually tunable reference cell." Optics Communications 535 (2023), Art. ID 129346. DOI 10.1016/j.optcom.2023.129346.
[25] Y. Du, D. Lu, Q. He, X. Fang, Sensitivity Improvement in Vernier-Effect Demodulation Based on Frequency Doubling of Sensing Spectrum, IEEE Sens. J. 23 (2023) 5780–5785, https://doi.org/10.1109/JSEN.2023.3239195.
[26] C. Zhu, J. Huang, Self-Vernier Effect-Assisted Optical Fiber Sensor Based on Microwave Photonics and Its Machine Learning Analysis, J. Lightwave Technol. 41 (2023) 1890–1898, https://doi.org/10.1109/JLT.2022.3227247.
[27] X. Fang, C. Lin, M. Wan, D. Lu, S. Huang, J. Li, Z. Huang, W. Zhang, Ultrasensitive RI Sensing Based on the Signal-Processing-Assisted Vernier Effect of a Single FFPI, IEEE Photon. Technol. Lett. 34 (2022) 563–566, https://doi.org/10.1109/lpt.2022.3173506.
[28] Y. Guan, B. Yin, X. Dong, A High-Precision Method for the Determination of Cavity Length of a Fabry-Perot Interferometer, IEEE Photonics J. 14 (2022) 1–6, https://doi.org/10.1109/JPHOT.2022.3163282.
[29] Y. Jiang, Y. Yi, G. Brambilla, P. Wang, Ultra-high-sensitivity refractive index sensor based on dual-microfiber coupler structure with the Vernier effect, Opt Lett. 45 (2020) 1268, https://doi.org/10.1364/ol.385345.
[30] Y. Zhao, P. Wang, R. Lv, X. Liu, Highly Sensitive Airflow Sensor Based on Fabry-Perot Interferometer and Vernier Effect, J. Lightwave Technol. 34 (2016) 5351–5356, https://doi.org/10.1109/JLT.2016.2615054.
[31] Y. Yang, Y. Wang, Y. Zhao, J. Jiang, X. He, W. Yang, Z. Zhu, W. Gao, L. Li, Sensitivity-enhanced temperature sensor by hybrid cascaded configuration of a Sagnac loop and a F-P cavity, Opt Express. 25 (2017) 33290, https://doi.org/10.1364/oe.25.033290.
[32] L. Huang, G. Zhou, L. Yan, H. Yan, X. Jiang, Optical fiber Fabry-Perot interferometer refractive index sensor based on Vernier effect for silica colloidal sol aging monitoring, Opt. Fiber Technol. 60 (2020), https://doi.org/10.1016/j.yofte.2020.102338.
[33] H. Liao, P. Lu, X. Fu, X. Jiang, W. Ni, D. Liu, J. Zhang, Sensitivity amplification of fiber-optic in-line Mach-Zehnder Interferometer sensors with modified Vernier-effect, Opt Express. 25 (2017) 26898, https://doi.org/10.1364/oe.25.026898.
[34] Y. Li, Y. Li, Y. Liu, Y. Li, S. Qu, Detection Limitation Analysis of Optical Fiber Sensors Based on Interferometers with Vernier-effect, Opt Express. (2022), https://doi.org/10.1364/oe.469791.
[35] V.M.N. Passaro, B. Troia, F. de Leonardis, A generalized approach for design of photonic gas sensors based on Vernier-effect in mid-IR, Sens Actuators B Chem. 168 (2012) 402–420, https://doi.org/10.1016/j.snb.2012.04.044.
[36] C. Ma, E.M. Lally, A. Wang, Toward eliminating signal demodulation jumps in optical fiber intrinsic Fabry-Perot interferometric sensors, J. Lightwave Technol. 29 (2011) 1913–1919, https://doi.org/10.1109/JLT.2011.2144957.
[37] J.A. Flores-Bravo, M.A. Illarramendi, J. Zubia, J. Villatoro, Optical fiber interferometer for temperature-independent refractive index measuring over a broad range, Opt. Laser Technol. 139 (2021), 106977, https://doi.org/10.1016/j.optlastec.2021.106977.